

# node2coords: Graph Representation Learning with Wasserstein Barycenters

Effrosyni Simou<sup>1</sup>, Dorina Thanou<sup>2</sup>, and Pascal Frossard<sup>3</sup>

<sup>1,3</sup>Signal Processing Laboratory (LTS4), EPFL

<sup>2</sup>Swiss Data Science Center (SDSC), EPFL/ETHZ

## Abstract

In order to perform network analysis tasks, representations that capture the most relevant information in the graph structure are needed. However, existing methods do not learn representations that can be interpreted in a straightforward way and that are robust to perturbations to the graph structure. In this work, we address these two limitations by proposing node2coords, a representation learning algorithm for graphs, which learns simultaneously a low-dimensional space and coordinates for the nodes in that space. The patterns that span the low dimensional space reveal the graph’s most important structural information. The coordinates of the nodes reveal the proximity of their local structure to the graph structural patterns. In order to measure this proximity by taking into account the underlying graph, we propose to use Wasserstein distances. We introduce an autoencoder that employs a linear layer in the encoder and a novel Wasserstein barycentric layer at the decoder. Node connectivity descriptors, that capture the local structure of the nodes, are passed through the encoder to learn the small set of graph structural patterns. In the decoder, the node connectivity descriptors are reconstructed as Wasserstein barycenters of the graph structural patterns. The optimal weights for the barycenter representation of a node’s connectivity descriptor correspond to the coordinates of that node in the low-dimensional space. Experimental results demonstrate that the representations learned with node2coords are interpretable, lead to node embeddings that are stable to perturbations of the graph structure and achieve competitive or superior results compared to state-of-the-art methods in node classification.

## 1 Introduction

Data is often found to be in the form of a graph structure, like in citation networks or protein-protein interaction networks. Therefore, in order to perform network analysis tasks, for example node classification, it is necessary to design algorithms for the extraction of low-dimensional representations of graphs. This feature extraction process is challenging due to the irregularity of the data structure and has been addressed by employing frameworks from different fields, such as Spectral Graph Theory [1], Probability Theory [2] as well as tools from Natural Language Processing [3], for example. In this work we propose an algorithm for unsupervised learning of graph representations that leverages the mathematical theory of Optimal Transport.

Graph representation learning methods have two important limitations. First, even if their design is justified intuitively, they often do not lead to directly interpretable node embeddings. In particular, there is not a clear interpretation of the values in a node embedding vector. Second, they are highly unstable, as even small perturbations to the graph structure can lead to large changes in the embeddings learned [4]. As a result, small perturbations to the graph structure can lead, for example, to a large drop in accuracy in the task of node classification.

In this work, we address both limitations by proposing node2coords, an unsupervised learning algorithm that, given a graph structure, learns simultaneously a low-dimensional space as well as node coordinates in that space. Specifically, we propose an autoencoder architecture with a Wasserstein barycentric decoder. The input to the algorithm is given by node connectivity descriptors, which capture the local structure of the nodes. In the encoding step, the node connectivity descriptors pass through a linear layer followed by a softmax activation to obtain a small set of graph patterns. This small set of patterns define the low dimensional space and provide essentially a compressed version of the structural information in the graph. In the decoding step, each node connectivity descriptor is reconstructed as a Wasserstein barycenter of the small set of graph structural patterns that span the low-dimensional space. This step can be thought of as a “projection” of each node connectivity descriptor in the low dimensional space and it is achieved by learning its optimal barycentric coordinates [5] in that space. As a result, the value of each feature in the low-dimensional representation of a node can be interpreted as the proximity in terms of Wasserstein distance of the node connectivity descriptor to the

corresponding graph structural pattern. Furthermore, the node embeddings are robust to small perturbations of the graph structure.

Experimental results on real and synthetic data demonstrate that the node embeddings obtained with node2coords are stable with respect to small changes of the graph structure. Furthermore, we demonstrate that we achieve competitive or superior results in the tasks of community detection and node classification compared to state-of-the-art methods for unsupervised learning of node embeddings that leverage only the graph structure and not node features [6].

The structure of the paper is as follows. In Section 2 we review the related work in unsupervised learning of graph representations. In Section 3 we describe the mathematical framework of Optimal Transport that forms the basis of our algorithm. In Section 4 we present in detail our Wasserstein barycenter representation method, which is later proposed as a new layer in the decoder of our graph representation learning algorithm. We outline each block of node2coords in Section 5 and explain the interpretations of the graph representations it learns. The experimental evaluation of the performance of node2coords is provided in Section 6. Finally, we conclude and discuss the benefits of node2coords in Section 7.

## 2 Related Work

The design of algorithms that learn representations for graph structured data has been extensively researched in the last years. Such algorithms learn low-dimensional representations for the nodes of the graph that capture the most important information for inference on the graph. If these node embeddings are learned in order to be optimal for a specific downstream prediction task and use labeled data during training, such as the class to which nodes belong for the task of node classification for instance, the corresponding algorithm is a supervised graph representation learning algorithm. Otherwise, if patterns are being learned from the data with no pre-existing labels, it is an unsupervised graph representation learning algorithm. In the case where only the graph structure is being input to the learning algorithm, the node embeddings capture the most relevant structural information in the graph. However, if node features are also available, they can be leveraged by algorithms in order to learn embeddings that capture semantic information as well as the structural one.

We focus here on the methods that learn graph representations in an unsupervised manner and that have been designed to leverage only the graph structure as input, similarly to our algorithm. Such methods can be grouped into four categories, namely the distance-based methods, matrix factorization methods, skip-gram methods and autoencoders.

Distance-based embedding methods are algorithms that learn an embedding look-up by forcing nodes that are close in the graph to be mapped as close as possible in the embedding space with respect to a chosen distance metric. Notable methods in this category are Isomap [7], Locally Linear Embedding [8] and Laplacian Eigenmaps [9]. These algorithms capture the proximity of nodes on the graph via the geodesic distance, a linear approximation of local neighborhood of nodes and the smoothness of the eigenvectors of the Laplacian matrix of the graph respectively. These three methods measure similarity in the embedding space in terms of Euclidean distance.

Matrix factorization methods aim to learn low-rank representations of the adjacency matrix of a graph. The first such work is Graph Factorization [10] where an efficient algorithm is proposed for the factorization of large graphs. This is followed by HOPE [11] which proposes matrix factorization for directed graphs and GraRep [12] which allows for capturing higher order node proximities by leveraging powers of the adjacency matrix.

Skip-gram graph embedding methods are inspired by word embedding methods that use skip-gram [13] in order to predict context words for a given target word. Thus, by creating sequences of nodes, similarly to sentences of words, it is possible to learn embeddings by maximizing the probability of "context nodes". Sequences of nodes are generated using random walks and the obtained node sequences are fed to a skip-gram model which maximizes their log-likelihood and provides the node embeddings. In Deepwalk [14] a neural network is trained by maximizing the probability of predicting "context nodes" for each node of the graph. Node2vec [15] creates node sequences by generating biased random walks by combining Breadth First Search (BFS) and Depth First Search (DFS) and, as a result, learns node embeddings that capture similarities of nodes in terms of local structure as well as homophily. LINE [16] learns embeddings that preserve first-order and second-order node proximities.

Autoencoders for unsupervised learning of graph structures have an encoding and a decoding function that are composed of layers of linear functions and nonlinear activations, thus allowing for the learning of complex graph representations. Generally, the encoder takes as input the adjacency matrix of the graph and maps nodes to their low-dimensional embeddings. The decoder uses the low-dimensional embeddings to reconstruct the input. SDNE [17] is an autoencoder, which learns low-dimensional node embeddings that preserve first-order and second-order proximities. In order for this to be achieved, a regularizer that forces nodes that are connected on the graph to be close on the embedding space is added to the graph adjacency matrix reconstruction loss function. DNCR [18] creates a similarity matrix from the graph adjacency matrix using random surfing, which

is a probabilistic method that employs random walks. The obtained similarity matrix is fed to a denoising autoencoder in order to obtain the node embeddings.

Our proposed architecture is an autoencoder with a non-linear Wasserstein barycentric layer at the decoder. By introducing this geometry-aware, non-linear operation at the decoder, the graph representations learned have a clear interpretation and lead to stable node embeddings. Optimal Transport (OT) was also used for graph representation learning in DVNE [19] where they propose an autoencoder that maps nodes to Gaussian distributions in order to account for uncertainties in the graph structure and impose neighboring nodes to have a small Wasserstein distance between their corresponding Gaussians. This node embedding method, in terms of architecture, is an autoencoder composed of linear layers at the encoder and the decoder and only employs a Wasserstein-based loss at the objective function. In contrast, in node2coords we propose a new architecture for graph representation learning where the decoder directly employs elements from OT theory.

Finally, it is worth noting that OT ideas have been used for representation learning in different contexts. For example, in [20] the authors propose a dictionary learning algorithm for images where instead of the usual matrix product that determine dictionary and sparse codes, they propose to use Wasserstein barycenters for the image reconstruction. In [21] the authors propose a hierarchical optimal transport algorithm where they model documents as distributions over topics and use optimal transport distances to compare documents on the smaller topic space. In our work, we propose an autoencoder for graph representation learning that incorporates a novel Wasserstein barycentric layer at the decoder, which allows for geometry aware, non-linear combinations of graph patterns.

## 3 Preliminaries

### 3.1 Optimal Transport

Optimal Transport (OT) [22] is a mathematical theory that allows for the definition of geometry-aware distances between probability distributions. These distances take into account the geometry of the space on which the distributions are defined by leveraging a cost that captures the distances on that space.

The optimal transportation problem was first formulated by Monge [23] in order to find the optimal way to transport the entirety of the mass of a pile of sand to a different position. This problem was later relaxed by Kantorovich by allowing for split of mass during the transportation. The Kantorovich OT problem [24] aims to find a coupling  $\Gamma$ , where  $\Gamma(x, y)$  describes the probability of moving mass from  $x$  to  $y$ . In the discrete case where mass can only be found at specific positions, histograms can be considered and the geometry-aware cost is an  $n \times m$  matrix  $C$ , where  $n$  is the dimensionality of the source histogram  $I_0$  and  $m$  is the dimensionality of the target histogram  $I_1$ . The Kantorovich formulation of the OT problem is as follows:

$$K(I_0, I_1) = \min_{\Gamma \in \mathcal{U}(I_0, I_1)} \langle C, \Gamma \rangle \quad (1)$$

where:

$$\mathcal{U}(I_0, I_1) = \{\Gamma \in \mathbb{R}_+^{n \times m} : \Gamma \mathbf{1}_m = I_0 \text{ and } \Gamma^\top \mathbf{1}_n = I_1\} \quad (2)$$

is the polytope of transportation couplings that satisfy the mass preservation constraints and  $\mathbf{1}_n, \mathbf{1}_m$  are vectors of ones with dimension  $n$  and  $m$  respectively. The mass preservation constraints guarantee that the entirety of mass of the source  $I_0$  is transported to the target  $I_1$ .

The  $p$ -Wasserstein distance is defined as a specific case of the OT problem when  $n = m$ , and the cost matrix  $C$  in Eq. (1) can be expressed as the  $p$ -th elementwise power of the distance matrix  $D$  of the  $n$ -dimensional space. The  $p$ -Wasserstein distance is therefore obtained by:

$$W_p(I_0, I_1) = \left( \min_{\Gamma \in \mathcal{U}(I_0, I_1)} \langle D^p, \Gamma \rangle \right)^{1/p}. \quad (3)$$

### 3.2 Entropy Regularization

The problem in Eq. (3), (2) is a linear program and therefore can be solved with LP solvers such as the simplex algorithm [25]. In [26] the problem is regularized with the negative entropy of the coupling  $\Gamma$  and an efficient algorithm is proposed for its solution. The entropy-regularized Wasserstein distance is defined as:

$$\mathcal{W}_p^\epsilon(I_0, I_1) = \min_{\Gamma \in \mathcal{U}(I_0, I_1)} \langle C, \Gamma \rangle - \epsilon H(\Gamma) \quad (4)$$

where  $H(\Gamma) = -\sum_{i=1}^n \sum_{j=1}^n \Gamma(i, j) \log(\Gamma(i, j) - 1)$  is the entropy of the transportation coupling and  $\epsilon$  is the regularization parameter. This regularized problem can be solved efficiently with matrix scaling of the so-called Gibbs kernel  $K = e^{-\frac{C}{\epsilon}}$ . The Gibbs kernel is geometry aware, since it is a function of the cost  $C$ , but it is

also a non-negative matrix. The non-negativity of  $K$  leads to the efficient solution of the problem in Eq. (4), (2) using Sinkhorn’s matrix scaling algorithm [27]. Instead of the coupling  $\Gamma$ , the parameters that are being optimized in that case are the scaling vectors  $u$  and  $v$ , from which the coupling  $\Gamma$  can be eventually obtained as  $\Gamma = \text{diag}(u)K \text{diag}(v)$ . The solution of the problem in Eq. (4), (2) with  $L$  Sinkhorn iterations is shown in Algorithm 1:

---

**Algorithm 1** Sinkhorn Iterations for Wasserstein Distance

---

**Input:**  $I_0, I_1$

▷ Initialization

$$u^{(0)} = 1_N$$

**for**  $l \leftarrow 0$  to  $L - 1$  **do**

▷ Update first scaling vector

$$v^{(l)} = \frac{I_0}{K^\top u^{(l)}}$$

▷ Update second scaling vector

$$u^{(l+1)} = \frac{I_1}{K v^{(l)}}$$

$$\Gamma^{(L)} = \text{diag}(u^{(L)})K \text{diag}(v^{(L-1)})$$

**return**  $W_p^\epsilon(I_0, I_1) = \langle C, \Gamma^{(L)} \rangle$

---

In some cases it may be desired to relax the mass preservation constraints in order to compare a source  $I_0$  and a target  $I_1$  that do not have the same mass. In [28], it is proposed to control the mass variation through the parameter  $\rho$ , leading to the definition of the unbalanced Wasserstein distance with entropy regularization:

$$\begin{aligned} \mathcal{W}_p^{\epsilon, \rho}(I_0, I_1) = \min_{\Gamma \in \mathbb{R}_+^{N \times N}} & \langle C, \Gamma \rangle + \epsilon H(\Gamma) \\ & + \rho(\text{KL}(\Gamma 1_N | I_0) + \text{KL}(\Gamma^\top 1_N | I_1)), \end{aligned} \quad (5)$$

where  $\text{KL}(\cdot | \cdot)$  is the Kullback-Leibler divergence [29].

The problem in Eq. (5) can also be solved with Sinkhorn iterations as proposed in [28], equivalent to those in Algorithm 1. The only minor change necessary is the exponentiation of the scaling vectors  $u, v$  to  $\frac{\rho}{\rho + \epsilon}$  in order to ensure that the relaxed mass preservation constraints, as dictated by the value of  $\rho$ , are satisfied.

### 3.3 Wasserstein Barycenters

Given the Wasserstein distance, in [30] the notion of a Wasserstein barycenter of a set of histograms is introduced. The Wasserstein barycenter is an interpolation of  $S$  histograms  $\{I_k\}_{k=1}^S$  with weights  $\{\lambda_k\}_{k=1}^S$  and it is defined as:

$$\begin{aligned} \hat{b} = \underset{b}{\text{argmin}} & \sum_{k=1}^S \lambda_k W_p(I_k, b) \\ \text{subject to} & \sum_{k=1}^S \lambda_k = 1. \end{aligned} \quad (6)$$

The histogram  $\hat{b}$  is called the Wasserstein barycenter and the weights  $\{\lambda_k\}_{k=1}^S$  are referred to as barycentric coordinates.

In the specific case where the Wasserstein distance employed is the unbalanced Wasserstein distance of Eq. (5) the obtained barycenter is the unbalanced Wasserstein barycenter. Unbalanced Wasserstein barycenters [28] have been shown to better preserve the shape of the histograms  $\{I_k\}_{k=1}^S$  because erroneous mass does not have to appear in the barycenter in order to satisfy the mass preservation constraints.

When computing the barycenter of  $S$  histograms we are solving simultaneously  $S$  optimal transport problems between each of the  $S$  known targets, which are the  $S$  histograms  $\{I_k\}_{k=1}^S$ , and the unknown source, which is the barycenter  $b$ . Therefore, for the entropy-regularized case described above,  $S$  sets of scaling vectors  $u$  and  $v$  have to be computed. The computation of the unbalanced Wasserstein barycenter can be performed

through Sinkhorn iterations [31] as discussed in Section 3.2. An extra step is added for the estimation of the unknown barycenter  $b$ , which is needed for the update of the second scaling vectors. The solution of the entropy-regularized Wasserstein distance with Sinkhorn iterations is equivalent to the Kullback-Leibler (KL) [29] projection of the transportation coupling  $\Gamma$  to the convex sets defined by the mass preservation constraints [32]. The expression for the estimation of the unknown barycenter is derived from the first order conditions of the KL projections of the couplings to the convex sets defined by the mass preservation constraints of the known targets  $\{I_k\}_{k=1}^S$  [32]. The  $L$  Sinkhorn iterations for the computation of the unbalanced Wasserstein barycenter are shown in Algorithm 2.

---

**Algorithm 2** Sinkhorn Iterations for Unbalanced Wasserstein Barycenter

---

**Input:**  $\{I_k\}_{k=1}^S, \{\lambda_k\}_{k=1}^S$

▷ Initialization

**for**  $k \leftarrow 1$  to  $S$  **do**

$$u_k^{(0)} = 1_N$$

**for**  $l \leftarrow 0$  to  $L - 1$  **do**

▷ Update first scaling vectors

**for**  $k \leftarrow 1$  to  $S$  **do**

$$v_k^{(l)} = \left( \frac{I_k}{K^\top u_k^{(l)}} \right)^{\frac{\rho}{\rho+\epsilon}}$$

▷ Estimate Barycenter

$$b^{(l)} = \left( \sum_{k=1}^S \lambda_k (u_k^{(l)} \odot K v_k^{(l)})^{\frac{\epsilon+\rho}{\epsilon}} \right)^{\frac{\epsilon+\rho}{\epsilon}}$$

▷ Update second scaling vectors

**for**  $k \leftarrow 1$  to  $S$  **do**

$$u_k^{(l+1)} = \left( \frac{b^{(l)}}{K v_k^{(l)}} \right)^{\frac{\rho}{\rho+\epsilon}}$$

**return**  $\hat{b} = b^{(L-1)}$

---

## 4 Wasserstein Barycenters for Graph Representation Learning

In this section we propose a method for the parallel computation of multiple Wasserstein barycenters of graph patterns. This method is then employed in the barycentric layer of node2coords, where we introduce the idea of representing node connectivity descriptors, that capture the local structure of the nodes, as Wasserstein barycenters of a small set of basis graph patterns. We present our method for the efficient Wasserstein barycenter computation and analyse its complexity. Further, we provide an illustrative example of the non-linear, geometry aware interpolation of graph patterns obtained with Wasserstein barycenters and provide intuitions of why it was leveraged in our graph representation learning algorithm.

### 4.1 Efficient Method for Barycenter Computation of Graph Patterns

Given a graph  $G$  of  $N$  nodes with adjacency matrix  $\mathcal{A}$ , our method takes as input a matrix of  $S$  patterns on the graph  $M_S = [m_1, \dots, m_S]$ , with  $m_i$  an  $N \times 1$  graph pattern, and outputs their  $J$  Wasserstein barycenters  $B_J = [b_1, \dots, b_J]$ , as computed for  $J$  sets of barycentric coordinates  $\Lambda$  given by:

$$\Lambda = \begin{bmatrix} \lambda_{1,1} & \dots & \lambda_{1,S} \\ \dots & \dots & \dots \\ \lambda_{J,1} & \dots & \lambda_{J,S} \end{bmatrix}. \quad (7)$$

The barycenter  $b_i$  is an  $N$ -dimensional vector obtained as the barycenter of the graph patterns in  $M_S$  with weights  $\Lambda(i, \cdot) = [\lambda_{i,1}, \dots, \lambda_{i,S}]$ . Therefore, when learning graph representations with Wasserstein barycenters, the parameters being learned are the barycentric coordinates in  $\Lambda$ .

We propose to compute Wasserstein barycenters for patterns defined on a graph by taking into account the underlying graph geometry through the diffusion distance  $D_\tau$  [33]. Hence, the geometry aware cost  $C$  is chosen to be  $C = D_\tau^{\frac{1}{\epsilon}}$  and the Gibbs kernel becomes  $K = e^{-\frac{D_\tau}{\epsilon}}$ . The diffusion distance  $D_\tau$  captures the similarity of node connections in  $\tau$  hops and is computed using the  $\tau$ -th power of a Markov matrix  $P$  defining a random walk on the graph. For the graph  $G$  with adjacency matrix  $\mathcal{A}$ , the degree of node  $i$  is defined as:

$$d(i) = \sum_{j=1}^N \mathcal{A}(i, j) \quad (8)$$

and the Markov matrix  $P$  as:

$$P(i, j) = \frac{\mathcal{A}(i, j)}{d(i)}. \quad (9)$$

The diffusion distance  $D_\tau$  between a pair of nodes  $i, j$  is computed as:

$$D_\tau^2(i, j) = \|P^\tau(i, \cdot) - P^\tau(j, \cdot)\|_{L^2}^2 = \sum_{u=1}^N \frac{(P^\tau(i, u) - P^\tau(j, u))^2}{\pi(u)}$$

where:

$$\pi(x) = \frac{d(x)}{\sum_{y=1}^N d(y)}. \quad (10)$$

When two nodes  $i, j$  have similar connections in their  $\tau$ -hop neighborhood, the diffusion distance  $D_\tau(i, j)$  has a small value. The greater the difference of the  $\tau$ -hop connectivities of two nodes, the larger the value of their diffusion distance.

Given the Gibbs kernel  $K = e^{-\frac{D_\tau}{\epsilon}}$ , we can compute unbalanced Wasserstein barycenters with Sinkhorn iterations as presented in Section 3. However, as it can be seen from Algorithm 2, at each Sinkhorn iteration it is needed to update each of the  $S$  scaling vectors  $v$ , and then, once the barycenter has been estimated, update each of the  $S$  scaling vectors  $u$ . In the case where the updates of the  $S$  sets of scaling vectors are performed serially as in Algorithm 2, the computation of the barycenter is inefficient in terms of time complexity, because of the nested loops.

We avoid this increase in the time complexity with  $S$  by proposing a parallelized and computationally efficient method for the barycenter computation. Specifically, we update in parallel the  $S$  scaling vectors  $v$ . Then, after the barycenter estimation, we also update in parallel the  $S$  scaling vectors  $u$ . Our proposal for the efficient Wasserstein barycenter computation is demonstrated in Algorithm 3. An important element of the parallelization is due to the fact that the matrix-vector multiplications of the Gibbs kernel  $K$  with the scaling vectors  $u_k$  can be implemented in parallel as a matrix-matrix multiplication of the  $N \times N$  matrix  $K$  with the  $N \times S$  matrix  $U = [u_1, \dots, u_S]$  whose columns are the  $S$  scaling vectors  $\{u_k\}_{k=1}^S$ . Similarly, the matrix-vector multiplications of the matrix  $K$  with the  $S$  scaling vectors  $\{v_k\}_{k=1}^S$  can be implemented in parallel as a matrix-matrix multiplication of  $K$  with  $V = [v_1, \dots, v_S]$ . We now demonstrate step by step the computations of our proposed method for the computation of barycenters in parallel in Algorithm 3 and analyse their time complexity.

The first step is the update of the scaling vectors in  $V$ . In our implementation, the update of the  $S$  scaling vectors  $V$  is equivalent to the matrix multiplication  $K^\top U$ , the element-wise division of the  $N \times S$  matrices  $M_S$  and  $K^\top U$  and the elementwise exponentiation of the resulting  $N \times S$  matrix to  $\frac{\rho}{\rho + \epsilon}$ . The complexity for the update of the scaling vectors  $V$  is therefore  $\mathcal{O}(N^2S + 2NS)$ .

The second step is the estimation of the barycenter. We perform this update efficiently using matrix operations as:

$$B_J(i, \cdot)^{(l)} = (((1_N \otimes \Lambda(i, \cdot)) \odot (U \odot KV)^{\frac{\epsilon}{\epsilon + \rho}}) 1_S)^{\frac{\epsilon + \rho}{\epsilon}}. \quad (11)$$

The time complexity of this operation is  $\mathcal{O}(N^2S + 5NS + N)$ .

The third and final step is the update of the  $S$  scaling vectors  $U$ . This step is equivalent to the matrix multiplication  $KV$ , the element-wise division of the  $N \times S$  matrices  $B_J(i, \cdot) \otimes 1_S$  and  $KV$  and the elementwise exponentiation of the resulting  $N \times S$  matrix to  $\frac{\rho}{\rho + \epsilon}$ . Thus, the complexity for the update of the scaling vectors  $U$  is  $\mathcal{O}(N^2S + 3NS)$ .

As a result, the time complexity for our implementation of a Sinkhorn iteration of the barycenter  $B_J(i, \cdot)$  is  $\mathcal{O}(3N^2S + 10NS + N)$ , which means that it scales quadratically with respect to the number of nodes  $\mathcal{O}(N^2)$ . The  $J$  barycenters in  $B_J$  can be computed simultaneously using broadcasting operations, which are common in libraries such as PyTorch [34], and the complexity of each Sinkhorn iteration for the computation in parallel of

---

**Algorithm 3** Barycenter Computation in node2coords

---

**Input:**  $M_S, \Lambda(i, \cdot)$ 

▷ Initialization

$$U^{(0)} = 1_{N \times S}$$

**for**  $l \leftarrow 0$  to  $L - 1$  **do**

▷ Update first scaling vectors

$$V^{(l)} = \left( \frac{M_S}{K^\top U^{(l)}} \right)^{\frac{\rho}{\rho+\epsilon}}$$

▷ Estimate Barycenter

$$B_J(i, \cdot)^{(l)} = \left( \left( (1_N \otimes \Lambda(i, \cdot)) \odot (U \odot KV)^{\frac{\epsilon}{\epsilon+\rho}} \right) 1_S \right)^{\frac{\epsilon+\rho}{\epsilon}}$$

▷ Update second scaling vectors

$$U^{(l+1)} = \left( \frac{B_J(i, \cdot)^{(l)} \otimes 1_S}{KV^{(l)}} \right)^{\frac{\rho}{\rho+\epsilon}}$$

**return**  $B_J(i, \cdot)^{(L-1)}$ 

---

$J$  barycenters is  $\mathcal{O}(JN^2S)$ . Therefore, the overall complexity of the barycenter computation, which is composed of  $L$  Sinkhorn iterations, is  $\mathcal{O}(LJN^2S)$ . The number of Sinkhorn iterations  $L$  needed in order for the barycenter computation to converge increases as the entropy regularization parameter  $\epsilon$  decreases [35].

## 4.2 Illustrative Example of Wasserstein Barycenter of Graph Patterns

We now provide an illustration of the representations obtained with Wasserstein barycenters of graph patterns. Consider a graph composed of two clusters. Let  $m_1$  and  $m_2$  be two graph patterns, represented as non-negative valued functions on a graph, and localized at each cluster of the graph. The patterns  $m_1$ ,  $m_2$  as well as their unbalanced Wasserstein barycenter  $b$  for  $\lambda_1 = 0.2$  and  $\lambda_2 = 0.8$  are shown in Fig. (1). It can be seen that the barycenter  $b$  provides a non-linear, displacement interpolation of the patterns  $m_1$  and  $m_2$ . Also, the barycenter  $b$  has a larger support than the patterns  $m_1$  and  $m_2$  that are being interpolated because of the entropy regularization of Eq. (5). Specifically, as the value of the entropy regularization parameter  $\epsilon$  becomes larger, the barycenter tends to be uniform over the graph. Furthermore, the way the patterns are combined takes into account the underlying graph structure through the diffusion distance cost  $C = D_\tau$  and therefore Wasserstein barycenters provide geometry-aware non-linearities. It can also be seen that the values of the barycentric coordinates  $\lambda_1, \lambda_2$  quantify the proximity of the barycenter  $b$  with respect to the patterns  $m_1, m_2$ .

In our proposed graph representation learning algorithm, patterns similar to those illustrated in Fig. (1) are interpolated to obtain the Wasserstein barycenter approximation of node connectivity descriptors, that capture the local structure of the nodes. We note finally that the graph patterns that can be interpolated with Wasserstein barycenters are not restricted to be localized, as those shown in Fig. (1), but they can be any non-negative pattern on a graph. Thus, our proposed method can be integrated in different algorithms for learning representations of graph structured data by providing geometry aware, non-linear interpolations of graph patterns.

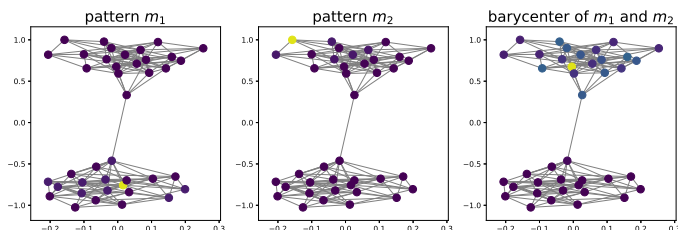


Figure 1: Localized graph patterns  $m_1, m_2$  and their Wasserstein barycenter interpolation for  $\lambda_1 = 0.2$  and  $\lambda_2 = 0.8$ .

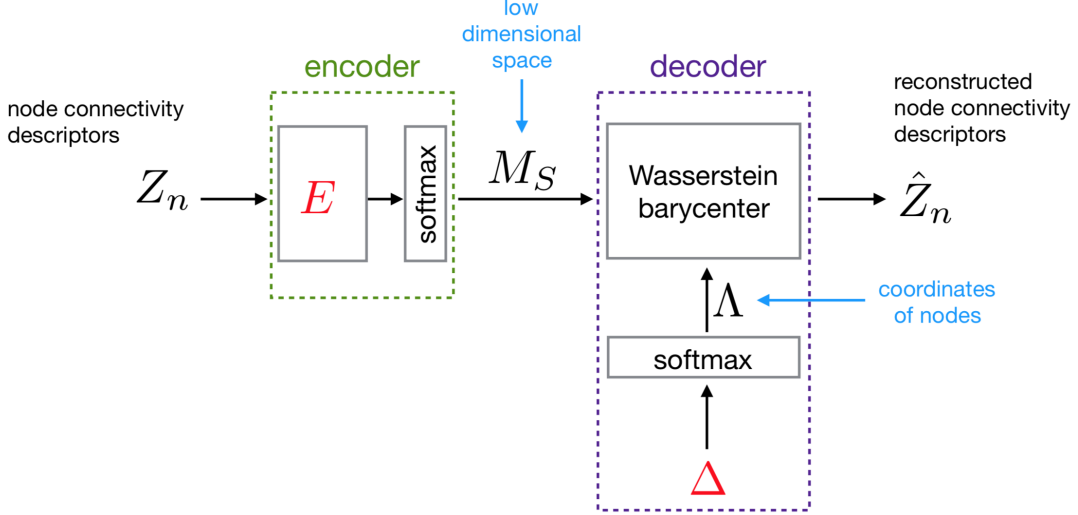


Figure 2: Node2coords block scheme. In the encoder, the node connectivity descriptors are passed through a linear layer followed by a softmax activation to obtain the small set of graph structural patterns that define the low dimensional space  $M_S$ . In the decoder, the node connectivity descriptors are reconstructed as Wasserstein barycenters of the patterns in  $M_S$  by optimizing for their barycentric coordinates  $\Lambda$ . The barycentric coordinates are re-parametrized through a softmax layer in order to guarantee that they sum up to one for each node. The learned parameters are the weights of the encoder  $E$  and the weights of the decoder  $\Delta$ , which are annotated with red.

## 5 node2coords

We present now node2coords, an unsupervised graph representation learning algorithm that relies on the graph Wasserstein barycenter representation method, introduced in Section 4. The proposed autoencoder architecture is shown in Fig. (2). The input of the encoder are the connectivity descriptors of the nodes  $Z_n$ , which capture their local structure. The node connectivity descriptors are passed through a linear layer followed by a softmax activation in order to obtain the small set of graph structural patterns  $M_S$ . In the decoder we employ Wasserstein barycenters as demonstrated in Section 4, to reconstruct the node connectivity descriptors as Wasserstein barycenters of the graph patterns in  $M_S$ . Thus, node2coords learns both the graph patterns  $M_S$  and the barycentric coordinates  $\Lambda$ . We give more details of each block of node2coords below.

**Input:** Given the adjacency matrix  $\mathcal{A}$  of a graph of  $N$  nodes, we choose to define the matrix of node connectivity descriptors  $Z_n$  as:

$$Z_n(i, j) = \frac{\tilde{\mathcal{A}}^n(i, j)}{\sum_{j=1}^N (\tilde{\mathcal{A}}^n(i, j))}. \quad (12)$$

The matrix  $\tilde{\mathcal{A}}$  is defined as  $\tilde{\mathcal{A}} = \mathcal{A} + \alpha \mathbb{I}_N$ , where  $\mathbb{I}_N$  is the  $N$ -dimensional identity matrix and  $\alpha \in \{0, 1\}$ . The matrix  $\tilde{\mathcal{A}}^n$  is therefore computed as  $\tilde{\mathcal{A}}^n = (\mathcal{A} + \alpha \mathbb{I}_N)^n$ . The  $i$ -th row  $Z_n(i, \cdot)$  is the connectivity descriptor of node  $i$  and its support indicates the nodes that can be reached from node  $i$  in up to  $n$  hops. The value of the parameter  $\alpha$  is set to  $\alpha = 0$  for  $n = 1$  because for  $n = 1$  the only nodes that can be reached from a node are its one-hop neighbors. However, for  $n \geq 2$  the value of  $\alpha$  is set to  $\alpha = 1$ . The reason for this choice is that for  $n \geq 2$ , a node can always reach itself by hopping to its first-hop neighbors and back. The value of the parameter  $n$  depends on the size of the graph  $G$ . Specifically, for larger values of the number of nodes  $N$ , larger values for  $n$  are required. An example of a connectivity descriptor for  $n = 1$  plotted on the graph is shown in Fig. (4).

**Encoder:** In the encoder, the node connectivity descriptors  $Z_n$  are passed through a linear layer with  $N \times S$  ( $S < N$ ) parameters  $E$  followed by a softmax activation. The  $N \times S$  matrix  $M_S$  obtained at the output of the encoder is therefore equal to:

$$M_S = \text{softmax}(Z_n E), \quad (13)$$

where the softmax activation of an  $N$ -dimensional vector  $x_i$  is defined as:

$$\text{softmax}(x_i) = \frac{e^{x_i}}{\sum_{j=1}^N e^{x_j}}. \quad (14)$$

The  $S$  patterns in  $M_S$  capture the most important structural properties of the graph and, therefore, we refer to them as graph structural patterns.



**Decoder:** In the decoder, the node connectivity descriptors in  $Z_n$  are reconstructed as Wasserstein barycenters of the  $S$  graph structural patterns in  $M_S$  using Wasserstein barycenters, as introduced in Algorithm 3. We obtain the optimal representations of the connectivity descriptors in  $\hat{Z}_n$  as Wasserstein barycenters of  $M_S$  by learning their barycentric coordinates  $\Lambda$ .

In order to guarantee that the barycentric coordinates of each of the barycenter representations sum up to one, we introduce a change of variable, through a softmax activation, so that the barycentric coordinates  $\Lambda(i, \cdot)$  of the barycenter approximation of the  $i$ -th node connectivity descriptor  $Z_n(i, \cdot)$  are reparametrized through a matrix  $\Delta$  as:

$$\lambda_{i,k} = \frac{e^{\delta_{i,k}}}{\sum_{j=1}^S e^{\delta_{i,j}}}. \quad (15)$$

The node connectivity descriptors in  $Z_n$  that are being approximated as Wasserstein barycenters at the decoder are localized in the  $n$ -hop neighborhood of the nodes. Therefore, their barycenter approximations in  $\hat{Z}_n$  are also localized in the  $n$ -hop neighborhood of the nodes. The localization of the barycenters in  $\hat{Z}_n$  in  $n$  hops, leads to learning patterns in  $M_S$  that are localized in up to  $n$ -hops. As the entropy regularization parameter  $\epsilon$  decreases, the patterns in  $M_S$  tend to be localized in exactly  $n$  hops. On the contrary, as  $\epsilon$  increases the patterns in  $M_S$  become more localized. Furthermore, in the Wasserstein barycentric layer of the decoder the graph is taken into account through the diffusion distance cost  $C = D_\tau^{p=1}$ . The nature of the displacement interpolation obtained with Wasserstein barycenters [36] and the use of the diffusion distance cost, which captures the geometry of the underlying graph, leads to a small set of patterns in  $M_S$  that highlight its structural properties.

It is important to observe that the decoding step can be thought of as an embedding of the nodes in the space spanned by the patterns in  $M_S$ . The  $i$ -th node of the graph, as described by its connectivity  $Z_n(i, \cdot)$ , is embedded in the  $S$ -dimensional space defined by the patterns in  $M_S$  by learning its  $S$ -dimensional coordinates  $\Lambda(i, \cdot)$ . As a result, each element of the  $S$ -dimensional embedding  $\Lambda(i, \cdot)$  of the node  $i$  quantifies the proximity, in terms of Wasserstein distance on the graph, of its connectivity descriptor to the  $S$  graph structural patterns.

**Optimization:** We train node2coords in order to learn the graph representations  $M_S$  and  $\Lambda$  by minimizing a loss  $\mathcal{L}(\hat{Z}_n, Z_n)$  between the node connectivity descriptors  $Z_n$  and their reconstruction as barycenters  $\hat{Z}_n$ . In order to ensure that the reconstruction of each node connectivity descriptor in  $Z_n$  is taken equally into account, we consider the normalized reconstruction loss:

$$\mathcal{L}(\hat{Z}_n, Z_n) = \frac{\|Z_n - \hat{Z}_n\|_F^2}{\|Z_n\|_F^2}. \quad (16)$$

It can be seen from Algorithm 3 and Eq. (15), (16) that  $\mathcal{L}(\hat{Z}_n, Z_n)$  is differentiable with respect to  $\Delta$  as well as with respect to  $M_S$ . Therefore,  $\mathcal{L}(\hat{Z}_n, Z_n)$  is differentiable with respect to  $\Delta$  and  $E$ . The minimization of the loss function is a non-convex problem:

$$\min_{E, \Delta} \frac{\|Z_n - \hat{Z}_n\|_F^2}{\|Z_n\|_F^2}, \quad (17)$$

that can be optimized with automatic differentiation [34] and stochastic gradient descent (SGD) [37]. The number of node connectivity descriptors that are being approximated as barycenters in parallel determines the batch size used for training with SGD. It can finally be noted that larger values of the entropy regularization  $\epsilon$  constitute the energy function in Eq. (17) less non-convex.

## 6 Experimental Results

### 6.1 Settings

In this section we evaluate the quality of the representations learned with node2coords for community detection, robust clustering and node classification tasks. We evaluate the performance of our algorithm against the following unsupervised learning methods:

- Laplacian Eigenmaps (LE) [9]: A shallow-embedding method that finds  $S$ -dimensional node embeddings by keeping the eigenvectors of the graph Laplacian matrix that correspond to the  $S$  smallest eigenvalues. LE embeddings naturally emphasize the clusters in the graph.
- DeepWalk [14]: An algorithm that uses random walks on graphs to learn  $S$ -dimensional representations of nodes with a skip-gram model.
- node2vec [15]: A skip-gram method that uses biased random walks on graphs allowing for a trade-off between homophily and structural equivalence of the obtained node embeddings.

- SDNE [17]: An autoencoder that learns  $S$ -dimensional node embeddings at the output of the  $N \times S$  linear layer of the encoder. SDNE embeddings preserve first-order and second-order node proximities.

The above methods were chosen in order to ensure comparison with benchmark methods as well as state-of-the-art methods for unsupervised learning of graph representations without node features.

## 6.2 Community Detection

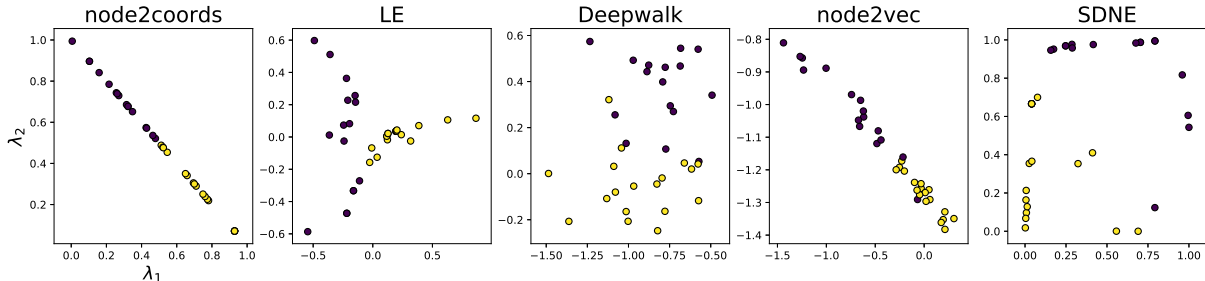


Figure 3: Embeddings obtained for the Zachary Karate network with node2coords, LE, Deepwalk, node2vec and SDNE. For node2coords the two axes correspond to the barycentric coordinates  $\lambda_1, \lambda_2$ . The embeddings of the other methods are not in a known coordinate system. The embeddings of the two communities are most clearly separated with node2coords.

We first evaluate the node embeddings learned by node2coords for the task of community detection on the Zachary Karate network [38]. We also take the opportunity to explain in detail the representations learned with node2coords and build intuitions on how to select optimally its parameters.

The Zachary Karate network is a common dataset used for the task of community detection. The network is composed of  $N = 34$  nodes. Each node is a member of a Karate university club, which is split into two communities.

We run node2coords for  $C = D_{\tau=1}$  and  $n = 1$  because the Karate network is a small graph and therefore 1-hop structural information is sufficient. We pick  $S = 2$  because there are two communities in the graph. For the remaining parameters, the values that led to the most clearly separable embeddings were  $\epsilon = 0.03$ ,  $\rho = 0.05$ . The choice of the value for the parameter  $\epsilon$  determines how localized the graph structural patterns will be and  $\rho$  controls the mass relaxation allowed. Furthermore,  $L = 500$  iterations were sufficient for the barycenter computation to converge. The input in node2coords is the connectivity matrix  $Z_{n=1}$  and the output is its reconstruction using barycenters  $\hat{Z}_{n=1}$ . We train using SGD with learning rate  $\mu = 0.01$ .

The graph structural patterns in  $M_S$  are shown in Fig. (5). It can be seen that the low-dimensional space  $M_S$  comprises two very localized structural patterns which are placed on the two communities. The embeddings obtained with node2coords are shown in Fig. (3). We can see that the two communities are perfectly separable. The values of the barycentric coordinates  $\lambda_1, \lambda_2$  of the nodes capture the proximity in terms of Wasserstein distance of the node connectivity descriptors, relatively to the graph structural patterns of  $M_S$ . As an example, the connectivity descriptor of the node in Fig. (4) is approximated in the decoder as  $\operatorname{argmin}_{u \in \Sigma_N} \sum_{i=1}^2 \lambda_i W_p^{\epsilon, \rho}(M_S(\cdot, i), u)$  where  $M_S(\cdot, 1), M_S(\cdot, 2)$  are the two patterns shown in Fig. (5) and  $\lambda_1 = 0.43, \lambda_2 = 0.57$  are the barycentric coordinates learned for that node. Therefore, the nodes that are close to the first pattern in  $M_S$  have a large  $\lambda_1$  and a small  $\lambda_2$ , as can be seen by the embeddings of the nodes in yellow in Fig. (3). The opposite is true for the nodes in the purple community.

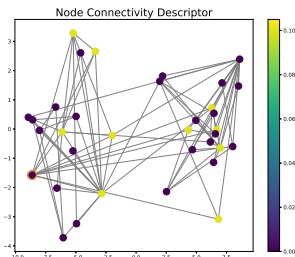


Figure 4: Connectivity descriptor of the node highlighted with the orange circle.

We also show in Fig. (3) the embeddings learned by Laplacian Eigenmaps, node2vec, DeepWalk and SDNE for latent dimensionality  $S = 2$  for the Zachary Karate Network. For node2vec, the parameters  $p, q$  are set to

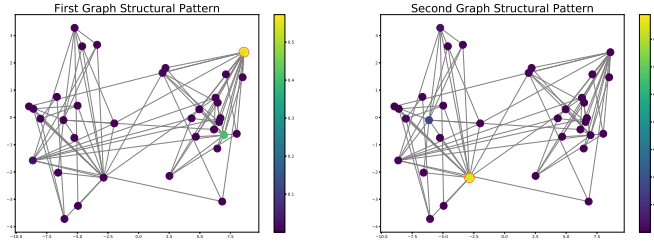


Figure 5: Graph structural patterns learned in  $M_S$  for the Zachary Karate network. The colormap shows the range of intensities of the pattern on the graph. The patterns learned in  $M_S$  are placed on each one of the communities.

$p = 1, q = 0.5$  which were proposed as optimal in [15] for the task of community detection where homophily among nodes is detected. For the remaining algorithms we optimize for the parameters in order to produce the most separable embeddings. For Deepwalk the number of walks is set to  $\gamma = 10$ , the walk length to  $t = 10$  and the window size to  $w = 3$ . For SDNE, the regularization for the first order proximities is equal to  $\alpha = 0.16$ , the  $L_2$  norm regularizer to avoid overfitting equal to  $\nu = 0.15$  and the reconstruction penalization parameter is set to  $\beta = 5$ . It can be seen that the embeddings obtained with all competitor unsupervised methods do not separate the two communities as clearly as node2coords. Furthermore, they lack interpretability as the value of the embedding of a node in each one of the two dimensions does not correspond to the proximity to a particular axes. In contrast, for node2coords the 2-dimensional space is spanned by the patterns shown in Fig. (5) which are localized in each community.

### 6.3 Stability to Perturbations

We now examine the stability of the representations learned with node2coords to perturbations of the graph structure. Specifically, we consider a stochastic block model [39] graph  $G$  of  $N = 100$  nodes with probability of connection within the community equal to  $p = 0.4$  and probability of inter-community connection equal to  $q = 0.01$ . We then consider perturbed versions  $G'$  of the graph  $G$  by varying the probability  $p$  within the range  $p' = \{0.15 : 0.05 : 0.40\}$ . Therefore, the perturbation affects the number of edges of the graph, but the number of nodes remains constant.

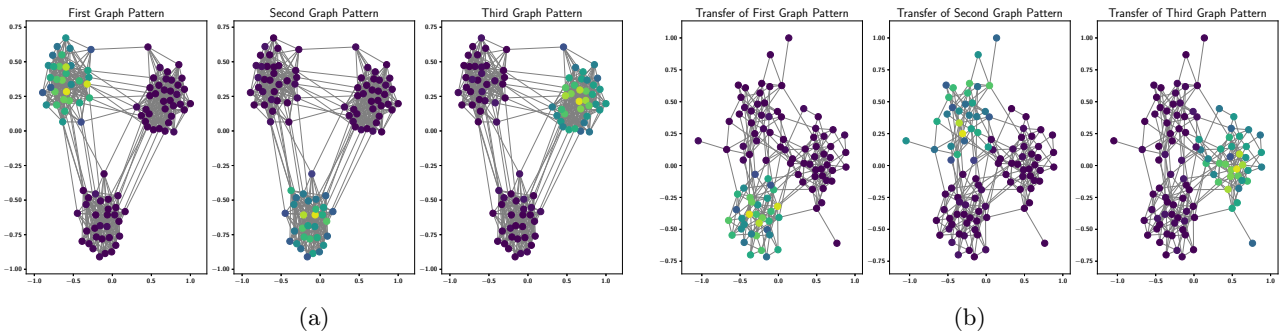


Figure 6: (a) Structural graph patterns of  $M_S$  as learned for the graph  $G$  with  $p = 0.4$ . Each pattern identifies one of the communities. (b) Structural graph patterns of  $M_S$  learned for the graph  $G$  with  $p = 0.4$  transferred to the perturbed graph  $G'$  with  $p' = 0.15$ . The graph structural patterns remain meaningful for the perturbed graph  $G'$  as they clearly indicate the three communities.

We run node2coords with  $n = 1, S = 3, \epsilon = 0.01$  and  $\rho = 0.1$  and learn the space  $M_S$  and the barycentric coordinates  $\Lambda$  for the graph  $G$ . The graph structural patterns learned in  $M_S$  for the clean graph  $G$  are shown in Fig. (6a) and their transfer to the perturbed graph  $G'$  with  $p' = 0.15$  in Fig. (6b). It can be seen that the graph patterns in  $M_S$  identify the three communities and thus they remain meaningful even when the actual graph changes. As a result, the perturbed graphs can be embedded in the low-dimensional space  $M_S$  that was learned for the clean graph  $G$ . We confirm this intuition by evaluating the clustering result obtained using the node embeddings  $\Lambda'$  of the perturbed graphs in the space  $M_S$  learned for the original graph  $G$ . For the perturbed graphs  $G'$  we only compute the barycentric coordinates  $\Lambda'$  of their nodes in the space  $M_S$  learned on  $G$ . In order to do so, we keep the weights of the encoder to be fixed and equal to those learned for the graph  $G$ , and we train only the barycentric weights in the decoder of node2coords. We apply  $k$ -means clustering to the barycentric coordinates of the nodes  $\Lambda'$  with  $k = 3$  and we compute the adjusted mutual information (AMI) and the normalized mutual information (NMI) [40] for the clustering result. The obtained AMI, NMI for the

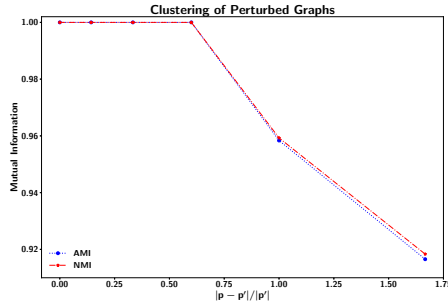


Figure 7: AMI and NMI scores as a function of the relative change of the probability of connection within the community  $\frac{|p-p'|}{|p'|}$ .

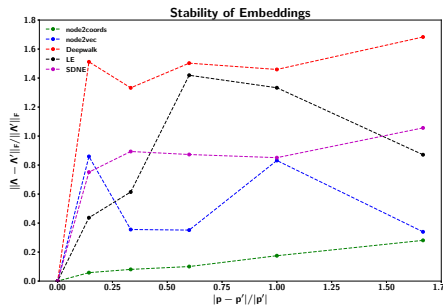


Figure 8: Relative change of the embeddings  $\frac{\|\Lambda - \Lambda'\|_F}{\|\Lambda'\|_F}$  as a function of the relative change of the probability of connection within the community  $\frac{|p-p'|}{|p'|}$ .

different perturbations are shown in Fig. (7). It can be seen that both the AMI and NMI are high even for large perturbations. Thus, we confirm that the perturbed graphs  $G'$  can be embedded in a meaningful way in the space  $M_S$  learned for the clean graph  $G$ .

We further evaluate the relative change  $\frac{\|\Lambda - \Lambda'\|_F}{\|\Lambda'\|_F}$  in terms of Frobenius norm of the barycentric coordinates  $\Lambda'$  of the perturbed graphs  $G'$  in comparison to the barycentric coordinates  $\Lambda$  of the original graph  $G$ . In Fig. (8) we show the relative change of the embeddings obtained as a function of the relative change of the probability of connection within the community  $\frac{|p-p'|}{|p'|}$ . Laplacian Eigenmaps, node2vec, Deepwalk and SDNE do not learn a low-dimensional space as node2coords and, therefore, the only way to obtain the node embeddings of the perturbed graphs is by re-running the algorithms.

It can be seen clearly that the embeddings obtained with node2coords are stable. Furthermore, the relative change in the embeddings seems to increase linearly with the relative change in the probability of intra-connection  $p$ . This is also clearly seen in Fig. (9) where we plot the node embeddings for node2coords. It can be seen that node embeddings obtained with node2coords change progressively as the value of the probability of connection  $p$  changes. The advantage of the stability of the embeddings with node2coords is due to the fact that the low-dimensional space  $M_S$  allows for stable embeddings and permits a registration of the nodes in the case of perturbed graphs. On the contrary, the other node embedding methods do not produce stable embeddings and the relative change in their embedding does not follow a clear trend as small changes in the structure can lead to big changes in the embeddings.

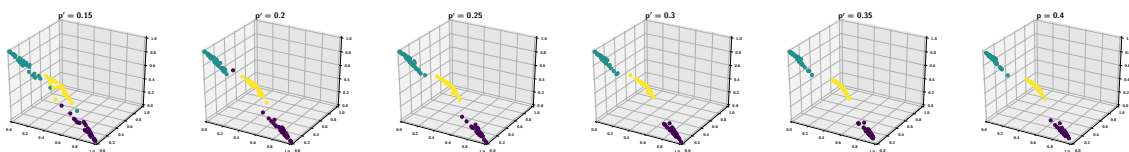


Figure 9: Embeddings of node2coords of the perturbed graphs  $G'$  in the space  $M_S$  learned for the clean graph  $G$ .

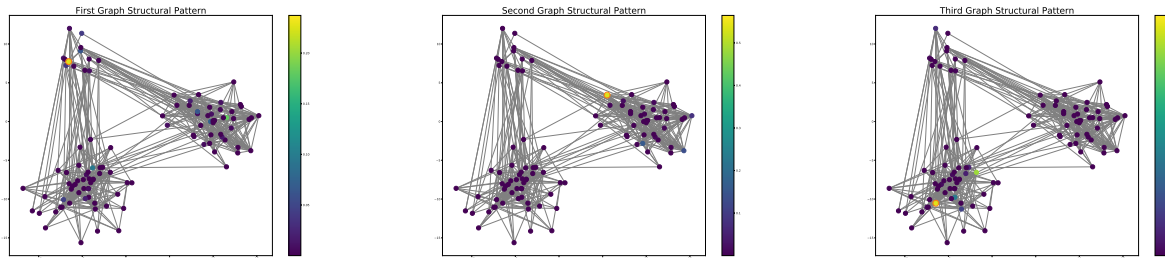


Figure 10: Graph structural patterns learned for PolBooks. The node with the highest value of each pattern is highlighted with an orange circle. Each graph structural pattern indicates a cluster of the graph.

## 6.4 Node Classification

We now evaluate the features learned in an unsupervised manner with node2coords in the context of node classification tasks. The node embeddings learned by node2coords and the competitor methods are input to a one-vs-rest logistic regression classifier with L2 regularization. The logistic regression classifier is a linear model commonly used for multi-label classification. The output of the thresholding of the linear combinations of its input features is inherently interpretable as the probability of a datapoint belonging to a class, and therefore, it is trained with the minimization of the cross-entropy loss. The L2 regularization is added to avoid overfitting to the training data.

For the node classification task we consider the following datasets:

- PolBooks: This dataset consists of a network of  $N = 105$  books about US politics published around the time of the 2004 presidential election and sold by the online bookseller Amazon.com [41]. Edges between books represent frequent copurchasing of books by the same buyers. The books belong to one of three classes “liberal”, “conservative”, “neutral”.
- Citeseer4: Citeseer [42] is a dataset that consists of a citation network extracted from the Citeseer digital library. Nodes are publications and an edge exists between two nodes if either publication has cited the other one. The publications belong to one of 6 classes, where each class corresponds to a research area. Citeseer4 is a network of  $N = 1532$  nodes and corresponds to the giant component of the network obtained by the publications that belong to the 4 research areas of the Citeseer network.

We consider train-test partitions of the data varying from 20% to 80%. For each partition we create 10 random splits of the data to train and test and provide results averaged over the 10 splits. For the evaluation of the classification results we compute the Macro-F1 score. The F1 score of a class is the harmonic mean of precision and recall. The precision for a class is the number of true positives divided by the total number of elements labeled as belonging to the class and recall is the number of true positives divided by the total number of elements that belong to the class. The Macro-F1 score is an unweighted mean of the F1 scores of each class.

We present in Table (1) the Macro-F1 scores for the PolBooks dataset and for train-test splits varying from 20% to 80%. For node2coords and the algorithms against which we evaluate its performance, the dimensionality of the embedding space is considered to be equal to  $S = 3$  as the network essentially has three clusters. It can be seen that node2coords provides the highest Macro-F1 score for most training ratios. Indeed, even for the small latent dimensionality of  $S = 3$ , it clearly identifies the small class “neutral”. This can be clearly seen also from the graph structural patterns of  $M_S$  in Fig. (10). Specifically, DeepWalk, node2vec and SDNE make most of the classification errors for the small class “neutral”, which leads to reduced Macro-F1 scores. This shows that the embedding dimensionality  $S = 3$  is too small for these algorithms to properly capture the three clusters in the data, while it is sufficient for node2coords.

We now examine how node2coords performs on larger datasets. We show in Table 2 the Macro-F1 scores for node classification on Citeseer4. The latent dimensionality for all methods is taken to be equal to  $S = 4$ . It can be seen again that node2coords provides the highest Macro-F1 scores for most train ratios. Therefore, node2coords is able to capture structural information for this larger graph. SDNE now has the second best performance, which shows that it is a method that scales well for large datasets. Also, node2vec performs consistently better than DeepWalk. This is due to the bias added to the random walks of node2vec, which leads to embeddings that capture both homophily as well as structural similarities of nodes. The worst performing method is LE, which does not scale well to larger graphs. The drop in performance of Laplacian Eigenmaps for large graphs could be due to the fact that it only takes into account first order proximities of the nodes. This is also indicated by the fact that the performance of SDNE, which takes into account second-order as well as first-order node proximities, improves for large graphs.

Table 1: Macro-F1 score for node classification in PolBooks.

<b>Train Ratio</b>	20%	30%	40%	50%	60%	70%	80%
LE	70.50	72.83	75.47	70.14	72.85	77.27	73.33
node2vec	72.48	<b>75.52</b>	74.77	70.80	73.61	80.76	<b>86.92</b>
DeepWalk	74.82	<b>75.52</b>	76.19	69.07	70.81	76.00	<b>86.92</b>
SDNE	64.48	65.40	68.65	70.65	70.81	72.22	79.16
node2coords	<b>75.58</b>	73.26	<b>78.43</b>	<b>73.58</b>	<b>78.88</b>	<b>86.11</b>	<b>86.92</b>

Table 2: Macro-F1 score for node classification in Citeseer4.

<b>Train Ratio</b>	20%	30%	40%	50%	60%	70%	80%
LE	30.78	32.47	31.81	32.87	34.09	34.57	36.63
node2vec	<b>68.56</b>	<b>69.97</b>	69.23	69.75	69.84	70.96	74.44
DeepWalk	57.56	59.61	59.01	59.18	59.10	60.69	60.27
SDNE	66.24	67.25	69.31	70.92	70.96	71.59	75.94
node2coords	66.94	68.63	<b>70.58</b>	<b>72.14</b>	<b>74.12</b>	<b>75.97</b>	<b>78.80</b>

## 6.5 Generalization to Unseen Nodes

In this experiment we evaluate the ability of node2coords to generalize to nodes that have not been seen during the representation learning process. In order to do so, we use only a downsampled version of the adjacency matrix of the PolBooks network during the representation learning process. Specifically, we use a randomly selected set of nodes for training and subsample the  $N \times N$  adjacency matrix  $\mathcal{A}$  to obtain the  $N^{train} \times N^{train}$  training adjacency matrix  $\mathcal{A}^{train}$ . From  $\mathcal{A}^{train}$  we obtain the training connectivity matrix  $Z_n^{train}$ . With  $Z_n^{train}$  as the input to node2coords, we learn the  $N^{train} \times S$  space  $M_S^{train}$  and the  $S$ -dimensional barycentric coordinates for each of the training nodes in that space. We eventually use the  $S$ -dimensional barycentric coordinates to train a one-vs-rest logistic regression classifier with L2 regularization.

As it has been shown above, the graph structural patterns learned with node2coords are sparse and they only have non-zero values on a small set of nodes within a given cluster. Therefore, we can upsample the patterns in  $M_S^{train}$  by zero padding in order to obtain the  $N \times S$  space  $M_S$ . The graph structural patterns in  $M_S$  obtained this way are meaningful as they indicate the clusters in the graph. We validate the quality of the patterns in  $M_S$  by evaluating the classification performance of the unseen nodes' coordinates in the space defined by  $M_S$ . Specifically, we compute the barycentric coordinates of the unseen, test nodes in the space  $M_S$  using the barycentric decoder of node2coords with fixed input  $M_S$ . We predict their class labels using the trained logistic regression classifier and evaluate the classification accuracy. We consider downsampling partitions ranging from 50 % to 90 %. For each partition we create 5 random splits of the data to train and test and provide results averaged over the 5 splits.

In Table (3) we show the classification accuracy for node2coords for downsampling ratios ranging from 50 % to 90 % (node2coords-DS) as well as the classification accuracy for the set-up of Section 6.4 (node2coords). We can see that the algorithm generalizes well to nodes that were completely unseen while learning the representation  $M_S$  with node2coords. When only 50 % of the nodes are kept in  $\mathcal{A}^{train}$  the classification accuracy for the nodes unseen during learning of  $M_S$  is 76.15 %.

Node2coords generalizes well to unseen nodes because the patterns learned for the downsampled graph capture the most important structural information which, in this case, corresponds to the clusters. This property is particularly useful in the case where the graphs under consideration are dynamic or temporally evolving. The ability of node2coords to learn such a meaningful low-dimensional representation of the graph, given only partial information of the graph structure, is unique to node2coords and cannot be reproduced by other methods for graph representation learning that only leverage structural information but not node features.

Table 3: Accuracy of node classification in PolBooks.

<b>Train Ratio</b>	50%	60%	70%	80%	90%
node2coords	86.79	90.47	93.75	95.23	100.00
node2coords-DS	76.15	76.19	78.06	83.80	80.00

## 7 Conclusion

In this work we proposed node2coords, an autoencoder architecture with a novel Wasserstein barycentric decoder that learns low-dimensional graph representations without supervision. The proposed algorithm learns simultaneously i) a low dimensional space and ii) node embeddings that correspond to coordinates in that space. The low-dimensional space is defined by a small set of graph patterns that capture the most relevant structural information of the graph. The values of a node’s embedding in that space can be interpreted as the proximity of its local connectivity to the corresponding graph patterns in terms of Wasserstein distance on the graph.

We demonstrated how the low-dimensional space of node2coords can be used to obtain significantly more stable embeddings for graphs that have undergone small perturbations, compared to other methods. Furthermore, we showed that the node embeddings of node2coords provide competitive or better results than those obtained with state-of-the-art methods for node classification tasks on real datasets. Finally, we confirm experimentally the ability to generalize to nodes that were unseen during the representation learning process, thus indicating the potential of node2coords to be used in dynamic settings with evolving graphs.

## References

- [1] F. R. Chung and F. C. Graham, *Spectral graph theory*. American Mathematical Society, 1997, no. 92.
- [2] E. T. Jaynes, *Probability theory: The logic of science*. Cambridge University Press, 2003.
- [3] C. Manning and H. Schütze, *Foundations of statistical natural language processing*. MIT press, 1999.
- [4] A. Bojchevski and S. Günnemann, “Certifiable robustness to graph perturbations,” in *Advances in Neural Information Processing Systems (NeurIPS)*, 2019, pp. 8317–8328.
- [5] N. Bonneel, G. Peyré, and M. Cuturi, “Wasserstein barycentric coordinates: histogram regression using optimal transport.” *ACM Transactions on Graphics*, vol. 35, no. 4, pp. 71–1, 2016.
- [6] I. Chami, S. Abu-El-Haija, B. Perozzi, C. Ré, and K. Murphy, “Machine learning on graphs: A model and comprehensive taxonomy,” *arXiv preprint arXiv:2005.03675*, 2020.
- [7] J. B. Tenenbaum, V. De Silva, and J. C. Langford, “A global geometric framework for nonlinear dimensionality reduction,” *Science*, vol. 290, no. 5500, pp. 2319–2323, 2000.
- [8] S. T. Roweis and L. K. Saul, “Nonlinear dimensionality reduction by locally linear embedding,” *Science*, vol. 290, no. 5500, pp. 2323–2326, 2000.
- [9] M. Belkin and P. Niyogi, “Laplacian eigenmaps and spectral techniques for embedding and clustering,” in *Advances in Neural Information Processing Systems (NIPS)*, 2002, pp. 585–591.
- [10] A. Ahmed, N. Shervashidze, S. Narayanamurthy, V. Josifovski, and A. J. Smola, “Distributed large-scale natural graph factorization,” in *Proceedings of the 22nd International Conference on World Wide Web*, 2013, pp. 37–48.
- [11] M. Ou, P. Cui, J. Pei, Z. Zhang, and W. Zhu, “Asymmetric transitivity preserving graph embedding,” in *Proceedings of the 22nd ACM SIGKDD International Conference on Knowledge Discovery and Data Mining*, 2016, pp. 1105–1114.
- [12] S. Cao, W. Lu, and Q. Xu, “Grarep: Learning graph representations with global structural information,” in *Proceedings of the 24th ACM International on Conference on Information and Knowledge Management*, 2015, pp. 891–900.
- [13] D. Guthrie, B. Allison, W. Liu, L. Guthrie, and Y. Wilks, “A closer look at skip-gram modelling.” in *Proceedings of the International Conference on Language Resources and Evaluation (LREC)*, vol. 6, 2006, pp. 1222–1225.
- [14] B. Perozzi, R. Al-Rfou, and S. Skiena, “Deepwalk: Online learning of social representations,” in *Proceedings of the 20th ACM SIGKDD international Conference on Knowledge Discovery and Data Mining*, 2014, pp. 701–710.
- [15] A. Grover and J. Leskovec, “node2vec: Scalable feature learning for networks,” in *Proceedings of the 22nd ACM SIGKDD International Conference on Knowledge Discovery and Data Mining*, 2016, pp. 855–864.
- [16] J. Tang, M. Qu, M. Wang, M. Zhang, J. Yan, and Q. Mei, “Line: Large-scale information network embedding,” in *Proceedings of the 24th International Conference on World Wide Web*, 2015, pp. 1067–1077.

- [17] D. Wang, P. Cui, and W. Zhu, “Structural deep network embedding,” in *Proceedings of the 22nd ACM SIGKDD International Conference on Knowledge Discovery and Data Mining*, 2016, pp. 1225–1234.
- [18] S. Cao, W. Lu, and Q. Xu, “Deep neural networks for learning graph representations,” in *AAAI Conference on Artificial Intelligence*, 2016.
- [19] D. Zhu, P. Cui, D. Wang, and W. Zhu, “Deep variational network embedding in wasserstein space,” in *Proceedings of the 24th ACM SIGKDD International Conference on Knowledge Discovery and Data Mining*, 2018, pp. 2827–2836.
- [20] M. A. Schmitz, M. Heitz, N. Bonneel, F. Ngole, D. Coeurjolly, M. Cuturi, G. Peyré, and J.-L. Starck, “Wasserstein dictionary learning: Optimal transport-based unsupervised nonlinear dictionary learning,” *SIAM Journal on Imaging Sciences*, vol. 11, no. 1, pp. 643–678, 2018.
- [21] M. Yurochkin, S. Claiçi, E. Chien, F. Mirzazadeh, and J. M. Solomon, “Hierarchical optimal transport for document representation,” in *Advances in Neural Information Processing Systems (NeurIPS)*, 2019, pp. 1601–1611.
- [22] C. Villani, *Optimal transport: old and new*. Springer Science & Business Media, 2008, vol. 338.
- [23] G. Monge, “Mémoire sur la théorie des déblais et des remblais,” *Histoire de l’Académie Royale des Sciences de Paris*, 1781.
- [24] L. Kantorovich, “On translation of mass,” *Doklady Akademii nauk SSSR*, vol. 37, pp. 227–229, 1942.
- [25] D. Goldfarb and J. K. Reid, “A practicable steepest-edge simplex algorithm,” *Mathematical Programming*, vol. 12, no. 1, pp. 361–371, 1977.
- [26] M. Cuturi, “Sinkhorn distances: Lightspeed computation of optimal transport,” in *Advances in Neural Information Processing Systems (NIPS)*, 2013, pp. 2292–2300.
- [27] P. A. Knight, “The sinkhorn–knopp algorithm: convergence and applications,” *SIAM Journal on Matrix Analysis and Applications*, vol. 30, no. 1, pp. 261–275, 2008.
- [28] L. Chizat, G. Peyré, B. Schmitzer, and F.-X. Vialard, “Scaling algorithms for unbalanced optimal transport problems,” *Mathematics of Computation*, vol. 87, no. 314, pp. 2563–2609, 2018.
- [29] S. Kullback and R. A. Leibler, “On information and sufficiency,” *The Annals of Mathematical Statistics*, vol. 22, no. 1, pp. 79–86, 1951.
- [30] M. Agueh and G. Carlier, “Barycenters in the wasserstein space,” *SIAM Journal on Mathematical Analysis*, vol. 43, no. 2, pp. 904–924, 2011.
- [31] H. Janati, M. Cuturi, and A. Gramfort, “Wasserstein regularization for sparse multi-task regression,” in *The 22nd International Conference on Artificial Intelligence and Statistics (AISTATS)*, 2019, pp. 1407–1416.
- [32] J.-D. Benamou, G. Carlier, M. Cuturi, L. Nenna, and G. Peyré, “Iterative bregman projections for regularized transportation problems,” *SIAM Journal on Scientific Computing*, vol. 37, no. 2, pp. A1111–A1138, 2015.
- [33] R. R. Coifman and S. Lafon, “Diffusion maps,” *Applied and Computational Harmonic Analysis*, vol. 21, no. 1, pp. 5–30, 2006.
- [34] A. Paszke, S. Gross, S. Chintala, G. Chanan, E. Yang, Z. DeVito, Z. Lin, A. Desmaison, L. Antiga, and A. Lerer, “Automatic differentiation in pytorch,” 2017.
- [35] A. Kroshnin, N. Tupitsa, D. Dvinskikh, P. Dvurechensky, A. Gasnikov, and C. Uribe, “On the complexity of approximating wasserstein barycenters,” in *International Conference on Machine Learning (ICML)*, 2019, pp. 3530–3540.
- [36] E. Simou and P. Frossard, “Graph Signal Representation with Wasserstein Barycenters,” in *IEEE International Conference on Acoustics, Speech and Signal Processing (ICASSP)*, 2019, pp. 5386–5390.
- [37] Y. A. LeCun, L. Bottou, G. B. Orr, and K.-R. Müller, “Efficient backprop,” in *Neural networks: Tricks of the trade*. Springer, 2012, pp. 9–48.
- [38] W. W. Zachary, “An information flow model for conflict and fission in small groups,” *Journal of anthropological research*, vol. 33, no. 4, pp. 452–473, 1977.



- [39] P. W. Holland, K. B. Laskey, and S. Leinhardt, “Stochastic blockmodels: First steps,” *Social networks*, vol. 5, no. 2, pp. 109–137, 1983.
- [40] N. X. Vinh, J. Epps, and J. Bailey, “Information theoretic measures for clusterings comparison: Variants, properties, normalization and correction for chance,” *The Journal of Machine Learning Research*, vol. 11, pp. 2837–2854, 2010.
- [41] *OrgNet*, 2004). [Online]. Available: <http://www.orgnet.com/divided2.html>
- [42] R. A. Rossi and N. K. Ahmed, “The network data repository with interactive graph analytics and visualization,” in *AAAI Conference on Artificial Intelligence*, 2015. [Online]. Available: <http://networkrepository.com>